



# Energy Absorption Performance of Bionic Multi-cell Tubes Inspired by Shrimp chela

Rui Liang<sup>1</sup> · Na Liu<sup>1</sup> · Xiang Liu<sup>1</sup> · Tao Wei<sup>1</sup> · Lirong Mo<sup>1</sup> · Huanchao Huang<sup>2</sup> · Christophe Bastien<sup>3</sup>

Received: 1 March 2023 / Revised: 26 June 2023 / Accepted: 26 June 2023 / Published online: 10 August 2023  
© The Chinese Society of Theoretical and Applied Mechanics 2023

## Abstract

This research introduced the design, analysis and optimization of bionic shrimp chela multi-cell tubes (BSCMTs) in bending by embedding an arthropod's microstructure inside a thin-walled square structure. A three-point impact bending finite element model was, in the first instance, correlated with physical tests and then modified to assess the energy absorption performance of bionic multi-cell tubes considering initial peak force, specific energy absorption and mean crushing force. Following a complex proportional assessment (COPRAS) approach and optimization phases, results demonstrated that the BSCMT with a W-shape section had the best energy absorption characteristics and should be considered in future as a possible contender for vehicle B-pillar structures that are subjected to bending and require excellent energy absorption properties to protect the occupants in high-speed impact collisions.

**Keywords** Energy absorption · Bionic · Microstructure · Shrimp chela · Multi-cell tube

## 1 Introduction

Outstanding energy absorption and lightweight characteristics offered by thin-walled structures (TWSs) make them ideal candidates for energy-absorbing components [1–3]. The early studies on TWSs primarily focused on hollow structures. For instance, Shojaeifard et al. [4] and Li et al. [5] established finite element (FE) models of circular and elliptical tubes based on experiments, then compared and analyzed their energy properties. Zhang et al. [6, 7] combined experiments and simulation methods to study the relationships between thickness and energy absorption responses. However, due to their relatively simple structures, these hollow TWSs cannot fully meet every industrial application. Consequently, foam-filled and carbon fiber reinforced polymer (CFRP)-reformed multi-cell tubes (MTs) were proposed and introduced to further improve the energy absorption performance of those energy-absorbing structures [8–10].

For example, Zhang et al. [11] performed bending tests on the embedded MTs, evidencing that 70% of the bending resistance was attributed to embedded MTs compared to traditional MTs. Besides, Huang et al. [12, 13] investigated the crashworthiness of the CFRP-enhanced MTs and found 7.9% higher specific energy absorption than the entirely wrapped tubes.

To date, bionic design has been another critical topic of interest to maximize the crashworthiness of tubes. Inspired by the microstructure of biomaterials, numerous studies have been conducted to improve the crashworthiness performance of MTs [14, 15]. Group studies of bionic multi-cell tubes (BMTs) were introduced based on vascular bundles [16, 17] and the diaphragm distribution of bamboo. Chen et al. [18–20], Zhou et al. [21], Duan et al. [22], Lam et al. [23], and Patek and Caldwell [24] systematically introduced a series of BMTs inspired by beetle forewings and shrimp chela. Their results indicated that the shrimp chela, a typical small-size biomaterial hammer, could withstand an impact force of up to 1500 N [24]. As a result, the bionic shrimp chela structure presents an interesting crashworthiness potential, and, as such, numerous BMTs inspired by shrimp chela have been made.

Guo et al. [25] developed double-layer structures based on the shrimp chela architecture. Yang et al. [26, 27] investigated the shrimp chela microstructure, established a series

✉ Na Liu  
naliu1989@126.com

<sup>1</sup> School of Automobile Engineering, Guilin University of Aerospace Technology, Guilin 541004, China

<sup>2</sup> Fangsheng Axle (Liuzhou) Co. LTD, Liuzhou 545036, China

<sup>3</sup> Institute for Future Transport and Cities, Coventry University, Coventry CV1 2TE, UK

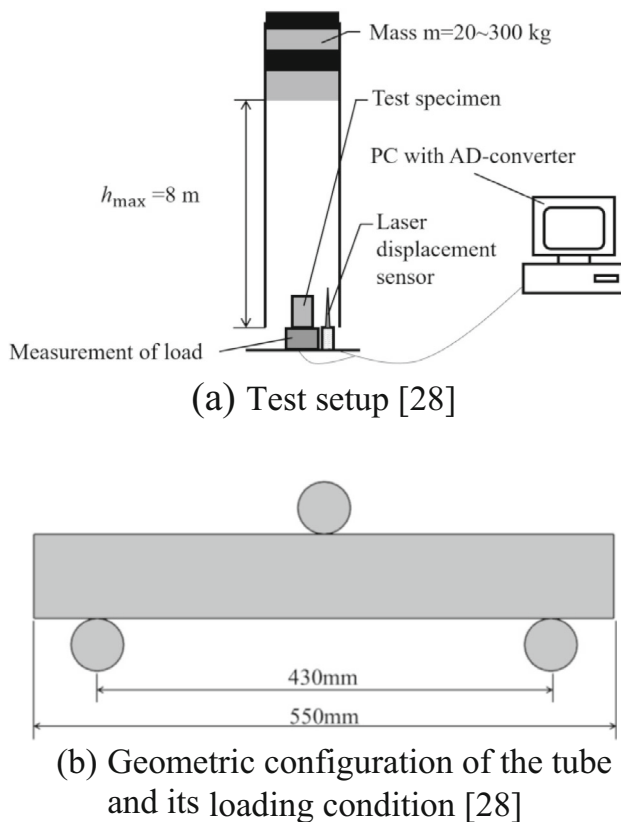


Fig. 1 Experiment detail

of BMTs, and employed a multi-objective optimization method to further improve their crashworthiness performance. Yang's results revealed that the optimal bionic shrimp chela multi-cell tubes (BSCMTs) presented 61.59% higher energy absorption. Therefore, applying bionic structures to design TWSs can be a novel approach to further improve energy absorption properties.

However, little research has been undertaken to study the energy absorption performance of BMTs inspired by shrimp chela subjected to impact bending. As a result, a novel study on BSCMTs, based on the structure of shrimp chela, is proposed in this paper, focusing on their ability to resist bending loads. The cross section, thickness parameters, multi-objective optimization design, and structure-enhanced design of the BSCMT are studied and proposed herein.

## 2 Methodology

### 2.1 Dynamic Experiment

Zarei and Kröge [28] conducted three-point bending experimental tests using the drop test rig (as shown in Fig. 1a) to calibrate the base finite element (FE) model. This experiment was instrumented to extract the strain, displacement and force

of the tubes. As presented in Fig. 1b, a hollow square tube (overall size: 55 mm × 55 mm × 550 mm) made of AA6060 aluminum alloy, was supported by two cylinders of 50 mm diameter placed 430 mm apart, and impacted by a cylinder of 50 mm diameter and 128 kg in the mid-span. This setup will serve as a qualitative reference for all the computational models and optimization processes in this paper.

## 2.2 Finite Element Modeling

### 2.2.1 Geometry and Material Description

The microstructure of the shrimp chela is depicted in Table 1, where continuous wavy V and W shapes can be observed. The study will therefore focus on the geometry of these V- and W-shaped BSCMTs and compare their dynamic energy absorption capabilities with those of the square tube, three-cell tube, and five-cell tube. Table 1 presents the cross sections of these five TWSs (overall size: 80 mm × 80 mm × 550 mm) made of AA6060 aluminum alloy, which has a density of  $2.7 \times 10^3 \text{ kg/m}^3$ , Young's modulus of 68.566 GPa, an initial yield stress is 227 MPa, Poisson's ratio of 0.29, and a tangential modulus of elasticity of 173 MPa [28, 29].

### 2.2.2 Finite Element Model

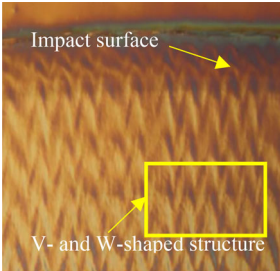
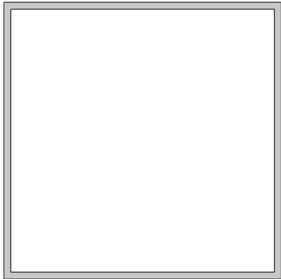
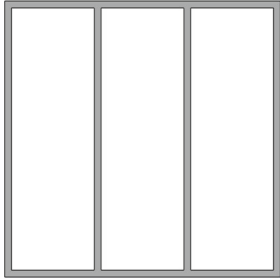

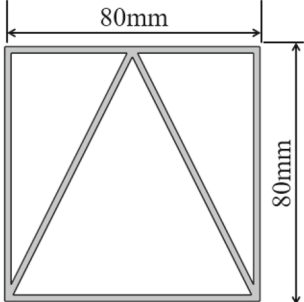
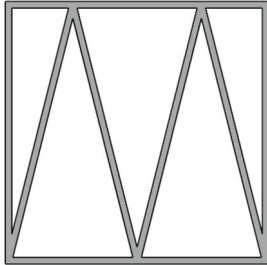
The nonlinear finite element code LS-DYNA was employed to create the FE models of BSCMTs, using 2 mm Belytschko–Lin–Tsay thin shell elements and a contact friction parameter of 0.2 between the BSCMTs, impactor and supports [7]. A \*MAT\_24 LS-DYNA material card was adopted to represent the properties of AA6060. Since aluminum is not sensitive to strain rate [31], the FE model omitted the rate-dependent effect. An initial impact velocity of 18 m/s (64 km/h) was chosen, which is higher than that in the experimental test conducted by Zarei and Kröge, to align with higher-speed vehicle test protocols.

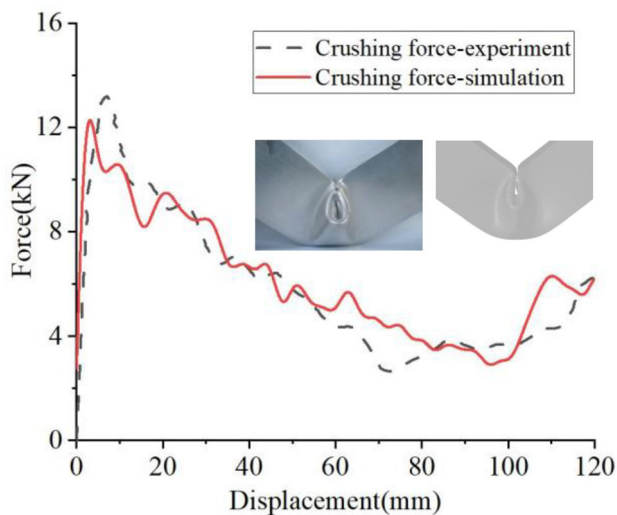
A BSCMT without a core would be a square tube. Thus, a square tube experiment established by Zarei and Kröge [28] was employed to calibrate the FE model, as shown in Fig. 2. The results revealed that the numerical force curve and deformation modes are in good agreement with the experimental results, demonstrating the correlation of the BSCMT FE model to reality.

### 2.3 Structural Energy Absorption Criteria

The most relevant criteria to evaluate energy absorption performance are the initial peak force (IPF), the specific energy absorption (SEA) and the mean crushing force (MCF) [32–34].

**Table 1** Macrostructure and microstructure of shrimp chela and the cross sections of five thin-walled tubes

Impact surface of the mantis shrimp and micrographs of the impact region [30]	Square tube	Three-cell tube
		
Five-cell tube	V-type BSCMT	W-type BSCMT
		



**Fig. 2** Comparison of crushing force versus displacement of the BSCMT between experiment [28] and simulation

The energy absorbed (EA) can be expressed as:

$$EA = \int_0^d F(x)dx \tag{1}$$

where  $d$  is the crushing distance, and  $F(x)$  denotes the crushing force at displacement  $x$ .

SEA is an essential criterion in lightweight design, as it represents the energy absorbed per unit mass and is defined as:

$$SEA = \frac{EA}{M} \tag{2}$$

where  $M$  is the total mass of the tube.

MCF is the mean crushing force, calculated as follows:

$$MCF = \frac{EA}{d} \tag{3}$$

### 2.4 Complex Proportional Assessment Method

The complex proportional assessment (COPRAS) uses a stepwise ranking method to evaluate design alternatives with respect to energy absorption performance [35–37]. The steps of the COPRAS method are described as [35–37]:

- Step 1: Define the initial decision matrix  $X$ .

$$X = [x_{ij}]_{mn} = \begin{bmatrix} x_{11} & x_{12} & \dots & x_{1n} \\ x_{21} & x_{22} & \dots & x_{2n} \\ \dots & \dots & \dots & \dots \\ x_{m1} & x_{m2} & \dots & x_{mn} \end{bmatrix} \tag{4}$$

where  $x_{ij}$  is the performance of the  $i$ th alternative on the  $j$ th criterion,  $m$  is the number of design alternatives, and  $n$  is the number of criteria.

- Step 2: Determine the non-dimensionalized matrix  $R$ .

A non-dimensionalized matrix  $R$  is denoted as:

$$R = [r_{ij}]_{mn} = \frac{x_{ij}}{\sum_{i=1}^m x_{ij}} \tag{5}$$

where the entry  $x_{ij}$  relates to the absolute value for each criterion, and  $\sum x_{ij}$  represents the summation for several positive decisions.

- Step 3: Fix the weighted normalized decision matrix  $D$ .

$$D = [y_{ij}]_{mn} = r_{ij} \times w_j \tag{6}$$

where  $r_{ij}$  represents the normalized performance value of the  $i$ th alternative on the  $j$ th criterion, and  $w_j$  is the weight of the  $j$ th criterion.

- Step 4: Define the weighted  $w_j$ .  $w_j$  could be defined as:

$$w_j = \frac{W_j}{G} \tag{7}$$

The total score of all criteria could be defined as:

$$G = \sum_{j=1}^n W_j \tag{8}$$

where the comparison sets ( $N$ ) are equal to  $N = (n(n-1)/2)$ , in which  $n$  is the number of selection criteria.

A BSCMT is expected to absorb as much impact energy per unit mass as possible [8], with the mean crushing force as high as possible to make the deformation more stable. SEA and MCF are considered to be more important than IPF. As a result, this paper assigns higher weightings to SEA and MCF and a lower one to IPF (0.42, 0.42, and 0.17, respectively).

The determination for the weight  $W_j$  of the  $j$ th criterion could be described as:

$$W_j = \sum_{i=1}^m N_{ij} \tag{9}$$

- Step 5: Sum the weighted beneficial and non-beneficial attributes.

$$S_+ = \sum_{i=1}^m S_{+i} = \sum_{i=1}^m \sum_{j=1}^n y_{+ij} \tag{10}$$

$$S_- = \sum_{i=1}^m S_{-i} = \sum_{i=1}^m \sum_{j=1}^n y_{-ij} \tag{11}$$

$$S_{-\min} = \min S_{-i} \tag{12}$$

where  $y_{+ij}$  and  $y_{-ij}$  are the beneficial and non-beneficial attributes, respectively, and  $S_{-\min}$  denotes the minimal value of  $S_{-i}$ .

In this paper, both SEA and CFE are identified as beneficial attributes that are preferred with a higher value, while the IPF is considered a non-beneficial attribute [38].

- Step 6: Determine the relative significance or priority  $Q_i$ .

$$Q_i = S_{+i} + \frac{S_{-\min} \sum_{i=1}^m S_{-i}}{S_{-i} \sum_{i=1}^m (S_{-\min}/S_{-i})} \tag{13}$$

A higher value of  $Q_i$  indicates a better design case.

- Step 7: Calculate the quantitative utility  $U_i$  for the  $i$ th alternative.

$$U_i = \frac{Q_i}{Q_{\max}} \tag{14}$$

where  $Q_{\max}$  is the maximum value of the relative significance or priority.

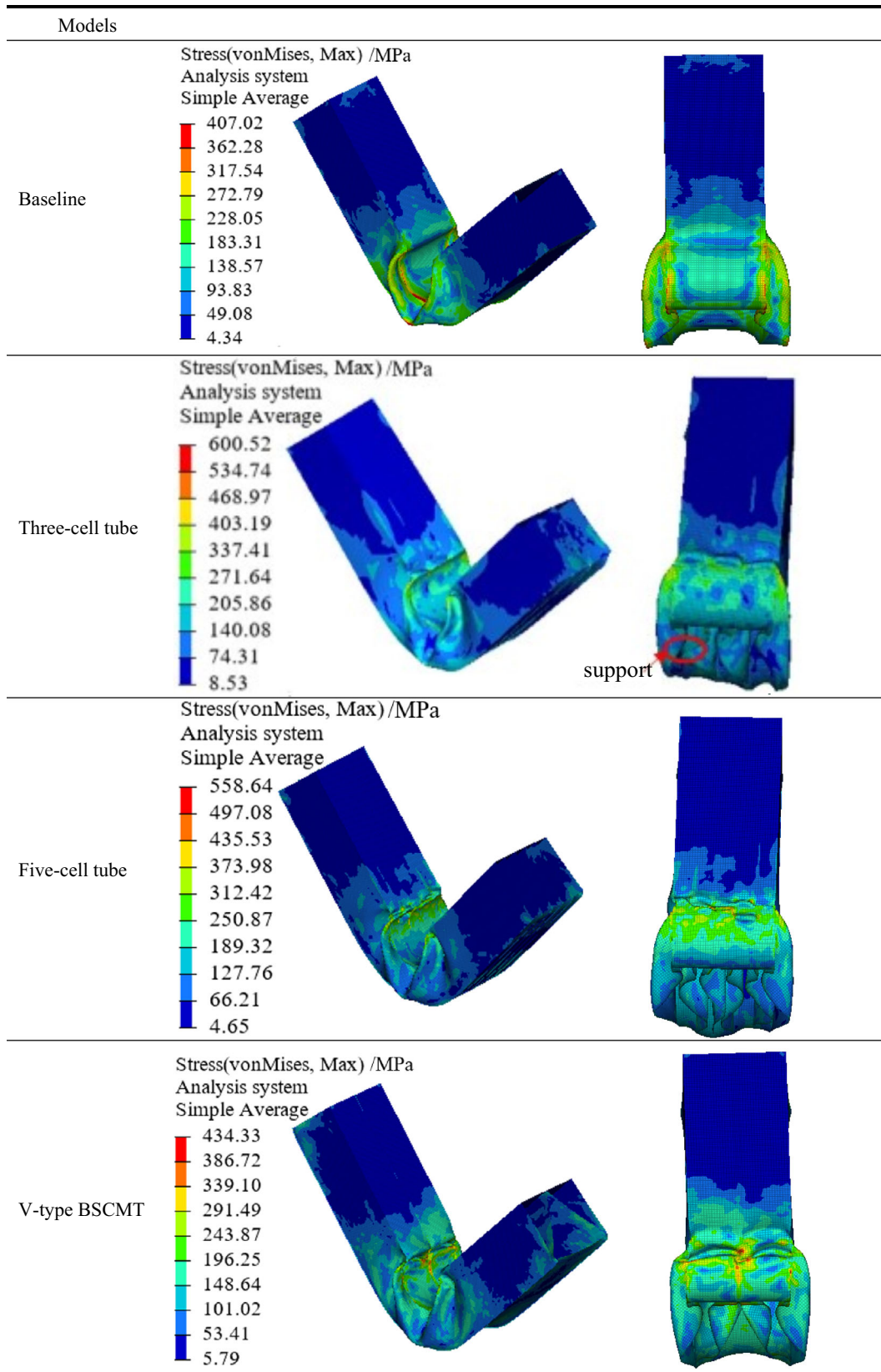
### 3 Results and Discussions

#### 3.1 Energy Absorption Properties

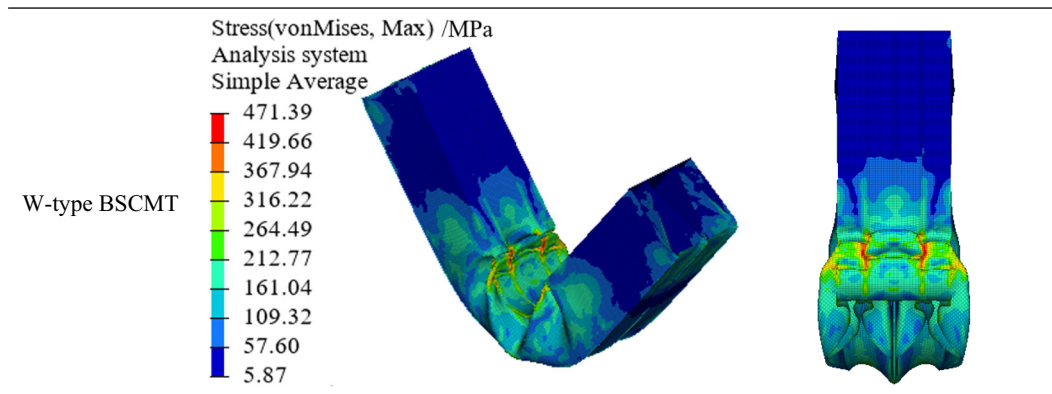
Table 2 depicts the stress contours of different TWSs at the maximum bending deformation. The cross section of the three-cell structure showed a contact between its internal diaphragm and the tube wall, indicating that only one side wall of the MT was supported by the internal diaphragm, resulting in an unstable slight axial deformation mode. In addition, Table 2 shows that the stress distribution in BSCMTs is generally more uniform compared to traditional MTs, making BSCMTs more efficient in energy absorption. Furthermore, it can be seen from the cross section view that BSCMTs have a higher stress concentration at the connection between the internal diaphragm and the tube wall compared to traditional MTs. Previous research [39] has also found that stress concentration at this connection could trigger a more progressive collapse deformation. As a result, BSCMT sections show more stable deformation modes.

Table 3 presents the energy absorption properties of different TWSs. The results reveal that, except for the W-type section, the BSCMTs' SEA does not show evident advantages over traditional MTs. However, by further observing Table 1, it is found that the BSCMT's internal diaphragm extends from the top to the bottom corner, making it longer than traditional MTs, and resulting in a slightly higher IPF than traditional MTs. As a result, to improve the performance of BSCMTs, it is necessary to focus on decreasing the IPF and increasing the SEA and MCF. The COPRAS method

**Table 2** Stress contours of various TWSs



**Table 2** (continued)



**Table 3** Weighted normalized decision matrix, beneficial and non-beneficial attributes,  $Q_i$  and  $U_i$

Models	IPF (kN)	SEA (kJ/kg)	MCF (kN)	$Q_i$	$U_i$ (%)	Rank
Baseline	25.31	3.99	11.18	0.14763	0.63069	5
Three-cell tube	44.95	6.48	30.76	0.20870	0.89157	3
Five-cell tube	67.46	6.58	43.00	0.23146	0.98879	2
V-type BSCMT	51.24	6.01	27.17	0.18813	0.80370	4
W-type BSCMT	74.97	6.81	43.60	0.23408	1	1

was employed to rank the crashworthiness response of these thin-walled tubes. The best design can be achieved when  $U_i$  equals one. According to the ranks given in Table 3, the W-type BSCMT is the most promising alternative among these thin-walled tubes. This section will be used in the following optimization.

### 3.2 Influence of Thickness on Energy Absorption Characteristic

The influence on energy absorption was investigated by varying the wall thickness  $t_1$  and the internal diaphragm thickness  $t_2$ . Sixty sample points were selected using the optimal Latin hypercube design (Opt LHD) method and were simulated. The results are graphed in Fig. 3, which demonstrate that the IPF, SEA and MCF significantly augment with the increases of  $t_1$  and  $t_2$ , indicating that thickness significantly affects energy absorption characteristics. In other words, if the wall thickness is taken as the minimum value, the minimum IPF can be obtained, but the SEA cannot reach its maximum at the same time. Besides, the slopes of IPF, SEA, and MCF, with respect to  $t_1$ , increase faster than those involving  $t_2$ , suggesting that the energy absorption performance of the BSCMT is more sensitive to  $t_1$ .

Moreover, the IPF, SEA and MCF reach the minimum when  $t_1$  and  $t_2$  are at a minimum. As a result, a larger value of  $t_1$  and  $t_2$  enhances SEA and MCF, while a greater thickness value negatively influences IPF. Furthermore, the maximum IPF, SEA, and MCF were recorded to be 121.55 kN, 7.41 kJ,

and 75.24 kN, respectively, suggesting that optimal values of wall thickness and internal diaphragm thickness can lead to better crashworthiness response. In summary, the wall thickness and internal diaphragm thickness significantly influence energy absorption capabilities. Reducing the thickness decreases IPF, SEA, and MCF. However, these cannot simultaneously reach the optimal solution. Therefore, further multi-objective optimization is required to obtain optimal structural energy absorption performance.

### 3.3 Optimization

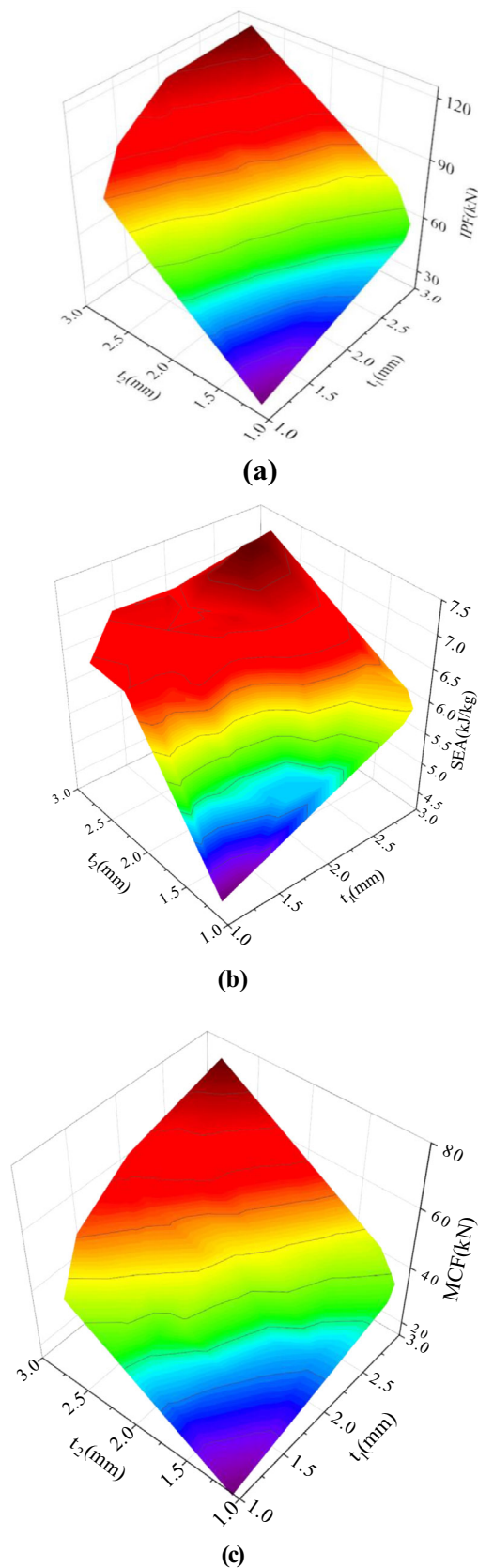
#### 3.3.1 Optimization Process

A multi-objective optimization method is adopted to select the optimal BSCMT with the lowest IPF, highest SEA, and MCF. A response surface methodology (RSM) is used to establish the approximation, while the NSGA-II algorithm is employed to optimize the thickness based on the RSM results.

#### 3.3.2 Optimization Results and Analysis

The correlation coefficient  $R^2$  and root-mean-square error (RMSE) are utilized as means to assess the approximations proposed by RSM:

$$R^2 = \frac{\sum_{i=1}^n (\hat{y}_i - \bar{y})^2}{\sum_{i=1}^n (y_i - \bar{y})^2} \tag{15}$$



**Fig. 3** Energy absorption characteristics of W-type BSCMT with different thicknesses: **a** IPF; **b** SEA; **c** MCF

$$\text{RMSE} = \sqrt{\frac{\sum_{i=1}^n (\hat{y}_i - y_i)^2}{n}} \quad (16)$$

where  $y_i$  is the  $i$ th real response value,  $\hat{y}_i$  is the  $i$ th predicted value,  $\bar{y}$  is the average value, and  $n$  is the number of sample points.

An accurate RSM is generated when  $R^2 > 0.9$  and  $\text{RMSE} < 0.2$ . The higher the  $R^2$  and the lower the RMSE, the greater the approximation reliability.

The relationships between the IPF, SEA, MCF, wall thickness ( $t_1$ ) and internal diaphragm thickness ( $t_2$ ) are

$$\text{IPF} = -17.1972 + 36.0639t_2 + 4.6225t_1^2 \quad (17)$$

$$\text{SEA} = 3.1709 + 0.1508t_1^2 + 1.4750t_2^2 - 0.3839t_2^3 \quad (18)$$

$$\text{MCF} = -13.3294 + 13.9796t_1 + 11.1911t_2^2 - 2.0454t_2^3 \quad (19)$$

The  $R^2$  values (0.99, 0.93, 0.99) for the IPF, SEA and MCF RSM models are all above 0.93, while the RMSE values (0.02, 0.07, 0.02) are all below 0.07. This indicates that the RSM models can reasonably predict the energy absorption response of the BSCMT and can be used in the following steps of the research.

A Pareto front is then obtained using the NSGA-II algorithm. By constraining the IPF to 75 kN (chosen as the arbitrary midpoint of the IPF value range [8]), a final compromise solution can be found. The final optimization results are listed in Table 4, which show relative errors of less than 5.5%. Furthermore, the energy absorption characteristics of IPF, SEA and MCF have improved by 3.64%, 11.63%, and  $-2.37\%$ , respectively, compared to the initial structure.

The optimization process has demonstrated that BSCMT structures can be optimized to generate superior energy absorption capabilities compared to standard cross sections. BSCMT could be used as a potential contender for B-pillar designs that are subjected to bending and high-speed impacts.

## 4 Conclusions

FE analysis was used to study the performance of BSCMTs subjected to bending load. BSCMTs were compared to square tubes and traditional MTs under the same three-point impact loading conditions to investigate their energy absorption characteristics. The results of the COPRAS method suggested that the W-type BSCMT had superior IPF, SEA, and MCF responses compared to standard sections, and wall thickness had a decisive influence on the crashworthiness performance. A multi-objective optimization method was

**Table 4** Comparison of optimized results

Variables	Initial structure	Optimized structure	Verification structure	Relative error (%)
$t_1$ (mm)	2.0	3.0	3.0	–
$t_2$ (mm)	2.0	1.4	1.4	–
IPF (kN)	74.965	74.895	72.240	3.545
SEA (kJ/kg)	6.811	6.366	6.019	5.451
MCF (kN)	43.600	44.931	44.608	0.719

employed on a W-type BSCMT section, which successfully minimized IPF and maximized SEA and MCF. Engineering experience has shown that in car collisions, the body in white (BIW) is prone to significant deformation due to lateral bending forces, which can harm occupants. Therefore, this new technology can have its place in vehicle design, especially as a new method for producing B-pillars to avoid excessive bending and protect passengers in side impact accidents.

## 5 Future Work

In future, more bionic multi-cell tubes will be investigated, considering the density of the chela and including the manufacturing processes of extrusion and 3D printing, which can have a constraint on the number of cells, as well as the structural response.

**Acknowledgments** This paper is supported by the 2022 Guangxi University Young and Middle-aged Teachers' Basic Research Ability Improvement Project (Grant No. 2022KY0781), Scientific Research Funds of Guilin University of Aerospace Technology (Grant No. XJ21KT18) and the Major Special Projects of Liuzhou Science and Technology Plan (Grant No. 2022ABA0106).

**Author contribution** RL contributed to investigation, writing—original draft, writing—review and editing, methodology, funding acquisition. NL contributed to data curation, supervision, project administration. XL contributed to data curation, funding acquisition. TW contributed to data curation, methodology. LM contributed to data curation, methodology. HH contributed to data curation, funding acquisition. CB contributed to writing—original draft, writing—review and editing.

**Data Availability** The datasets generated and/or analyzed during the current study are available from the corresponding author on reasonable request.

**Competing interests** The authors have no competing interests to declare that are relevant to the content of this article.

## References

- Zhang L, Bai Z, Bai F. Crashworthiness design for bio-inspired multi-cell tubes with quadrilateral, hexagonal and octagonal sections. *Thin-Walled Struct.* 2018;122:42–51.
- Huang H, Xu S. Crashworthiness analysis and bionic design of multi-cell tubes under axial and oblique impact loads. *Thin-Walled Struct.* 2019;144:106333.
- Niu X, Xu F, Zou Z. Bionic inspired honeycomb structures and multi-objective optimization for variable graded layers. *J Sandw Struct Mater.* 2022. <https://doi.org/10.1177/10996362221127969>.
- Shojaefard MH, Zarei HR, Talebitooti R, Mehdikhanlo M. Bending behavior of empty and foam-filled aluminum tubes with different cross-sections. *Acta Mech Solida Sin.* 2012;25:616–26.
- Li Z, Zheng Z, Yu J, Guo L. Crashworthiness of foam-filled thin-walled circular tubes under dynamic bending. *Mater Des.* 2013;52:1058–64.
- Zhang X, Zhang H, Ren W. Bending collapse of folded tubes. *Int J Mech Sci.* 2016;117:67–78.
- Zhang X, Zhang H, Wang Z. Bending collapse of square tubes with variable thickness. *Int J Mech Sci.* 2016;106:107–16.
- Yin H, Xiao Y, Wen G, Qing Q, Deng Y. Multiobjective optimization for foam-filled multi-cell thin-walled structures under lateral impact. *Thin-Walled Struct.* 2015;94:1–12.
- Yin H, Xiao Y, Wen G, Gan N, Chen C, Dai J. Multi-objective robust optimization of foam-filled bionic thin-walled structures. *Thin-Walled Struct.* 2016;109:332–43.
- Liu Q, Xu X, Ma J, Wang J, Shi Y, Hui D. Lateral crushing and bending responses of CFRP square tube filled with aluminum honeycomb. *Compos B Eng.* 2017;118:104–15.
- Zhang X, Zhang H, Leng K. Experimental and numerical investigation on bending collapse of embedded multi-cell tubes. *Thin-Walled Struct.* 2018;127:728–40.
- Huang Z, Zhang X. Crashworthiness and optimization design of quadruple-cell Aluminum/CFRP hybrid tubes under transverse bending. *Compos Struct.* 2020;235:111753.
- Huang Z, Zhang X, Yang C. Experimental and numerical studies on the bending collapse of multi-cell Aluminum/CFRP hybrid tubes. *Compos B Eng.* 2020;181:107527.
- Niu X, Xu F, Zou Z, Fang T, Zhang S, Xie Q. In-plane dynamic crushing behavior and energy absorption of novel bionic honeycomb structures. *Compos Struct.* 2022;299:116064.
- Jin M, Hou X, Yin G, Yao R, Gao J, Deng Z. Improving the crashworthiness of bio-inspired multi-cell thin-walled tubes under axial loading: experimental, numerical, and theoretical studies. *Thin-Walled Struct.* 2022;177:109415.
- Gao Z, Zhang H, Zhao J, Ruan D. The axial crushing performance of bio-inspired hierarchical multi-cell hexagonal tubes. *Int J Mech Sci.* 2023;239:107880.
- Sethi A, Budarapu PR, Vusa VR. Nature-inspired bamboo-spiderweb hybrid cellular structures for impact applications. *Compos Struct.* 2023;304:116298.
- Chen J, Dai G, Xu Y, Iwamoto M. Optimal composite structures in the forewings of beetles. *Compos Struct.* 2007;81:432–7.
- Chen J, Gu C, Guo S, Wan C, Wang X, Xie J, et al. Integrated honeycomb technology motivated by the structure of beetle forewings. *Mater Sci Eng C Mater Biol Appl.* 2012;32:1813–7.



20. Chen J, Dai G, Xu Y, Iwamoto M. Basic study of biomimetic composite materials in the forewings of beetles. *Mater Sci Eng A*. 2008;483–484:625–8.
21. Zhou M, Huang D, Su X, Zhong J, Hassanein MF, An L. Analysis of microstructure characteristics and mechanical properties of beetle forewings, *Allomyrina dichotoma*. *Mater Sci Eng C Mater Biol Appl*. 2020;107:110317.
22. Duan Y, Zhang T, Zhou J, Xiao H, Chen X, Al Teneiji M, et al. Energy-absorbing characteristics of hollow-cylindrical hierarchical honeycomb composite tubes inspired a beetle forewing. *Compos Struct*. 2021;278:114637.
23. Lam L, Chen W, Hao H, Li Z, Ha NS. Dynamic crushing performance of bio-inspired sandwich structures with beetle forewing cores. *Int J Impact Eng*. 2023;173:104456.
24. Patek SN, Caldwell RL. Extreme impact and cavitation forces of a biological hammer: strike forces of the peacock mantis shrimp *Odontodactylus scyllarus*. *J Exp Biol*. 2005;208:3655–64.
25. Guo X, Dong X, Yu Z, Zhang Z, Xie X, Wang X, et al. Study on the mechanical properties of bionic protection and self-recovery structures. *Materials*. 2020;13:389.
26. Yang X, Fan X, Xu S, Huang H, Huo P. Design and crashworthiness analysis of thin-walled tubes based on a shrimp chela structure. *Explos Shock Waves*. 2020;40(4):043301.
27. Huang H, Yan Q, Xiang Z, Yang X, Chen J, Xu S. Crashworthiness investigation and optimization of bionic multi-cell tube based on shrimp chela. *J Jilin Univ (Eng Technol Ed)*. 2022;52:716–24.
28. Zarei HR, Kröger M. Bending behavior of empty and foam-filled beams: structural optimization. *Int J Impact Eng*. 2008;35:521–9.
29. Yin H, Chen C, Hu T, Wen G. Optimisation for bending crashworthiness of functionally graded foam-filled cellular structure. *Int J Crashworthiness*. 2017;23:446–60.
30. Yang X, Ma J, Shi Y, Sun Y, Yang J. Crashworthiness investigation of the bio-inspired bi-directionally corrugated core sandwich panel under quasi-static crushing load. *Mater Des*. 2017;135:275–90.
31. Hou S, Li Q, Long S, Yang X, Li W. Crashworthiness design for foam filled thin-wall structures. *Mater Des*. 2009;30:2024–32.
32. Bigdeli A, Nouri MD. A crushing analysis and multi-objective optimization of thin-walled five-cell structures. *Thin-Walled Struct*. 2019;137:1–18.
33. Li Z, Chen R, Lu F. Comparative analysis of crashworthiness of empty and foam-filled thin-walled tubes. *Thin-Walled Struct*. 2018;124:343–9.
34. Pirmohammad S, Marzdashti SE. Crushing behavior of new designed multi-cell members subjected to axial and oblique quasi-static loads. *Thin-Walled Struct*. 2016;108:291–304.
35. Chatterjee P, Chakraborty S. Material selection using preferential ranking methods. *Mater Des*. 2012;35:384–93.
36. Chatterjee P, Athawale VM, Chakraborty S. Materials selection using complex proportional assessment and evaluation of mixed data methods. *Mater Des*. 2011;32:851–60.
37. Zavadskas EK, Turskis Z, Tamošaitiene J, Marina V. Multicriteria selection of project managers by applying grey criteria. *Ukio Technol Ekon Vystym*. 2008;14:462–77.
38. Sun G, Liu T, Huang X, Zheng G, Li Q. Topological configuration analysis and design for foam filled multi-cell tubes. *Eng Struct*. 2018;155:235–50.
39. Xu F, Yu K, Hua L, Niu X. Crashworthiness design of crash box filled with negative Poisson's ratio based on horn structure. *Mech Adv Mater Struct*. 2022;29(27):6403–20.

Springer Nature or its licensor (e.g. a society or other partner) holds exclusive rights to this article under a publishing agreement with the author(s) or other rightsholder(s); author self-archiving of the accepted manuscript version of this article is solely governed by the terms of such publishing agreement and applicable law.